

Nonlinear analysis of flexodomains in nematic liquid crystals

Werner Pesch*

Physikalisches Institut, Universität Bayreuth, 95440 Bayreuth, Germany

Alexei Krekhov†

Max Planck Institute for Dynamics and Self-Organization, 37077 Göttingen, Germany

Nándor Éber and Ágnes Buka

Institute for Solid State Physics and Optics, Wigner Research Centre for Physics, Hungarian Academy of Sciences, H-1525 Budapest, P.O. Box 49, Hungary

(Received 19 June 2018; published 5 September 2018)

We investigate flexodomains, which are observed in planar layers of certain nematic liquid crystals, when a dc voltage U above a critical value U_c is applied across the layer. They are characterized by stationary stripelike spatial variations of the director in the layer plane with a wave number $p(U)$. Our experiments for different nematics demonstrate that $p(U)$ varies almost linearly with U for $U > U_c$. That is confirmed by a numerical analysis of the full nonlinear equations for the director field and the induced electric potential. Beyond this numerical study, we demonstrate that the linearity of $p(U)$ follows even analytically, when considering a special parameter set first used by Terent'ev and Pikin [Sov. Phys. JETP **56**, 587 (1982)]. Their theoretical paper serves until now as the standard reference on the nonlinear analysis of flexodomains, since it has arrived at a linear variation of $p(U)$ for large $U \gg U_c$. Unfortunately, the corresponding analysis suffers from mistakes, which in a combination led to that result.

DOI: [10.1103/PhysRevE.98.032702](https://doi.org/10.1103/PhysRevE.98.032702)**I. INTRODUCTION**

In the last decades, pattern-forming instabilities induced by electric fields in nematic liquid crystals (nematics) have been intensely studied both in theory and experiments; for a recent review see Ref. [1]. Nematics are anisotropic liquids without translational, but with long-range orientational order of their elongated molecules. That order is described by the director field $\mathbf{n}(\mathbf{r})$, which obeys the normalization condition $\mathbf{n}^2 = 1$. The crucial ingredient for the understanding of electrically driven instabilities in nematics is the uniaxial anisotropy of all their material parameters, which thus depend on the local orientation of \mathbf{n} [2]. In the past, so-called electroconvective instabilities have been mostly studied, where the electrical conductivity of the nematic liquid crystal plays an important role. One deals then with dissipative systems, where the instabilities are associated with charge separation and flow fields, which are tightly coupled to \mathbf{n} .

In the present paper we concentrate, however, on insulating (dielectric) nematics, where in contrast to dissipative systems, the thermal equilibrium state corresponds to a minimum of a free energy. That contains, first, a term describing the orientational elasticity against director variations, characterized by three elastic constants k_{ii} , $i = 1, 2, 3$. Second, there exists a dielectric contribution with two dielectric permittivities, ϵ_{\parallel} and ϵ_{\perp} , for the electric field parallel and perpendicular

to \mathbf{n} , respectively. Finally, the so-called *flexoelectric* effect is crucial, which means that spatial variations of \mathbf{n} lead to an electric polarization (flexopolarization). There is a certain analogy to piezoelectricity, where mechanical deformations of various solids produce an electric polarization as well. The flexopolarization couples to the applied electric field and gives a contribution to the free energy, which is characterized by the two flexocoefficients e_1 and e_3 (for recent reviews, see Refs. [3,4] and references therein).

In the following, we deal with the so-called *planar* configuration, where a thin nematic layer of thickness d is sandwiched between two confining plates parallel to the x, y plane at $z = \pm d/2$. The plates serve two purposes. First, they are used as electrodes to apply a dc voltage U to the nematic layer. Second, the plates are specially treated to enforce a fixed orientation of \mathbf{n} parallel to the x axis at the surface. Due to the orientational elasticity of nematics, this configuration is uniformly present over the whole layer for zero and small U . However, for certain favorite combinations of the dielectric constants, the elastic ones, and the flexocoefficients, one observes instead for U above a critical voltage U_c the so-called *flexodomains*, which present a periodic array of the director distortions along the y direction with wave number p [5]. By exploiting the optical anisotropy of nematics, the flexodomains can be identified by optical means (diffraction, shadowgraphy) when light is transmitted through the layer. It should be noted, that flexodomains can be easily distinguished from the intensely examined electroconvection rolls, where \mathbf{n} varies periodically in the x direction.

*werner.pesch@uni-bayreuth.de

†alexei.krekhov@ds.mpg.de

The theoretical analysis of flexodomains is based on the exploration of the absolute minimum of the free energy. For values of $U < U_c$ the minimum corresponds to the uniform planar basic state and for $U > U_c$ to the flexodomains, which continuously bifurcate at $U = U_c$ from the basic state with the critical wave number p_c . A detailed analysis of the threshold quantities U_c and p_c can be found in the literature (see, e.g., Refs. [6–8]). The main goal of the present paper is the theoretical description of the flexodomains in the *nonlinear* regime for $U > U_c$, where the minimal free energy is realized by flexodomains with wave number $p = p_{\min}(U)$.

To our best knowledge, the only theoretical analysis of $p_{\min}(U)$ has been presented in the paper of Terent'ev and Pikin [9] for $U \gg U_c$. Their study is restricted to a substantially simplified version of the general equations, which is characterized by two different aspects. First, they used a special “isotropic” material parameter set assuming the one-elastic-constant approximation ($k_{ii} = k_{av}$), equal dielectric permittivities ($\epsilon_{\parallel} = \epsilon_{\perp}$), and $e_1 + e_3 = 0$. Second, the inevitable correction $\phi(\mathbf{r})$ to the electric potential in the nonlinear regime has been simply neglected without any comment. We will refer to the whole simplification scheme as the Terent'ev-Pikin approximation (TPA) throughout this paper.

In general, the basic equations for flexodomains can be mapped to a system of coupled partial differential equations for $\mathbf{n}(y, z)$ and $\phi(y, z)$. The problem vastly simplifies under the TPA and one arrives analytically at a constant slope of $p_{\min}(U)$ for $U > U_c$. The analysis remains still quite simple when using a less strict version of the TPA, where the induced potential ϕ is taken into account. In fact, one arrives at the same slope of $p_{\min}(U)$ as before except for some modifications in the vicinity of U_c .

A constant slope of $p_{\min}(U)$, though only for $U \gg U_c$, has been also obtained in the original analysis of Ref. [9], which, however, disagrees with our value. In Ref. [9] additional, not justified approximations beyond the TPA have been used. However, after correcting some additional technical errors in their work, we have been unable to obtain a linear behavior of $p_{\min}(U)$ at all.

The analysis of flexodomains using the TPA serves certainly as a first important step to understand the qualitative features of flexodomains in the nonlinear regime. But certainly one would like to compare the exact solutions of the basic equations for more realistic material parameters with experiments. However, experimental studies of the nonlinear behavior of flexodomains are not so often found in the literature; we are only aware of Refs. [10–14]. One finds here indeed a linear behavior of $p(U)$ with a reference to Ref. [9].

Since the material parameters of the nematics used in these papers are not well known, a conclusive theoretical analysis is prohibited. Thus, we have performed our own experiments using several nematics with well-known material parameters. As before, $p(U)$ shows a fairly linear behavior, and it was very satisfying that the slopes of $p(U)$ would match well our corresponding theoretical values of $p_{\min}(U)$.

The paper is organized as follows. After this introduction, the basic equations are discussed in Sec. II. Their linear stability analysis, which yields the critical voltage U_c , at which the flexodomains with critical wave number p_c bifurcate from

the homogeneous planar ground state, is sketched in Sec. III. The properties of the flexodomains in the nonlinear regime for $U > U_c$ using the TPA material parameters restrictions are analyzed in Sec. IV. In Sec. V we present our experiments on flexodomains for four different nematics and compare with corresponding theoretical results. After some concluding remarks in Sec. VI, several appendices deal with technical details and contain further supplementary information.

II. BASIC EQUATIONS

The nematic liquid crystal layer considered in this paper is assumed to have a very large lateral extension in the x, y plane compared to its thickness d , where the director $\mathbf{n} = \mathbf{n}_0 = (1, 0, 0)$ is uniform in the basic state. When a dc voltage $U = E_0 d$ is applied to the layer in the z direction, the corresponding electric field $\mathbf{E}_0 = E_0 \mathbf{e}_z$ exerts a torque on the director. If \mathbf{E}_0 is sufficiently strong to overcome the stabilizing elastic torques, flexodomains appear, which are characterized by spatially periodic distortions of \mathbf{n}_0 and of \mathbf{E}_0 . The resulting field \mathbf{E} is irrotational and is described by the ansatz:

$$\mathbf{E} = E_0 \mathbf{e}_z - \nabla \phi, \quad (1)$$

where the unit vectors $\mathbf{e}_x, \mathbf{e}_y, \mathbf{e}_z$ span our coordinate system and $-\nabla \phi$ yields the nonlinear correction to \mathbf{E}_0 . As demonstrated below, it is indeed sufficient to consider only $E_0 > 0$. Since U is kept fixed, ϕ vanishes at the confining plates, i.e., $\phi(z = \pm d/2) = 0$.

The total free energy, F_{tot} , of the system is obtained from the volume integral, $F_{\text{tot}} = \int d^3 \mathbf{r} \mathcal{F}_{\text{tot}}$ of the total free energy density, \mathcal{F}_{tot} , which is defined as follows:

$$\mathcal{F}_{\text{tot}} = \mathcal{F}_d + \mathcal{F}_{\text{el}} - \lambda(\mathbf{r})(\mathbf{n} \cdot \mathbf{n} - 1), \quad (2)$$

where \mathcal{F}_d describes the orientational elasticity of nematics and \mathcal{F}_{el} the electric contribution. By the Lagrange parameter $\lambda(\mathbf{r})$ the normalization $\mathbf{n}^2 = 1$ is guaranteed. The standard expression for \mathcal{F}_d is given as follows:

$$\mathcal{F}_d = \frac{1}{2} [k_{11}(\text{div } \mathbf{n})^2 + k_{22}(\mathbf{n} \cdot \text{curl } \mathbf{n})^2 + k_{33}(\mathbf{n} \times \text{curl } \mathbf{n})^2]. \quad (3)$$

The three elastic constants, k_{11}, k_{22}, k_{33} , correspond to the splay, twist, and bend director deformations, respectively. The electric part, \mathcal{F}_{el} , which depends on the two relative dimensionless dielectric permittivities $\epsilon_{\perp}, \epsilon_{\parallel}$ with the dielectric anisotropy $\epsilon_a = \epsilon_{\parallel} - \epsilon_{\perp}$ and on the flexocoefficients e_1, e_3 is given as

$$\mathcal{F}_{\text{el}} = -\frac{1}{2} \epsilon_0 [\epsilon_{\perp} (\mathbf{E}^2 - \mathbf{E}_0^2) + \epsilon_a (\mathbf{n} \cdot \mathbf{E})^2] - \mathbf{E} \cdot \mathbf{P}_{\text{fl}}, \quad (4)$$

with the flexopolarization

$$\mathbf{P}_{\text{fl}} = e_1 \mathbf{n}(\text{div } \mathbf{n}) + e_3 (\mathbf{n} \cdot \nabla) \mathbf{n}, \quad (5)$$

where $\epsilon_0 = 8.8542 \times 10^{-12}$ V s/(A m) denotes the vacuum permittivity. According to Landau-Lifshitz (p. 11 in Ref. [15]), \mathcal{F}_{el} (marked with a tilde there) is the appropriate free energy density in the presence of an external electric field \mathbf{E} acting on the nematic. This case is realized in the experiments, where the U is treated as fixed. The term $\frac{1}{2} \epsilon_0 \epsilon_{\perp} \mathbf{E}_0^2$ in Eq. (4) has been added to ensure that \mathcal{F}_{el} , as well as \mathcal{F}_{tot} vanish

in the uniform basic state $\mathbf{n} = \mathbf{n}_0$, $\mathbf{E} = \mathbf{E}_0$. Furthermore, \mathcal{F}_{tot} is invariant against the simultaneous transformations $\mathbf{E} \rightarrow -\mathbf{E}$ and $e_i \rightarrow -e_i$. Thus, the case $U < 0$ can be mapped to $U > 0$ by simply reversing the sign of the e_i .

A necessary condition for thermodynamic equilibrium states of our system is the vanishing of the functional derivatives $\delta F_{\text{tot}}/\delta \mathbf{n}$ and $\delta F_{\text{tot}}/\delta \mathbf{E}$ of F_{tot} with respect to \mathbf{n} and \mathbf{E} (for details see Appendix A). For the derivative with respect to \mathbf{n} we obtain thus:

$$\mathbf{h}(\mathbf{r}) - \lambda(\mathbf{r})\mathbf{n} = \mathbf{0}, \quad (6)$$

with

$$\mathbf{h}(\mathbf{r}) = \frac{\delta \int d^3\mathbf{r}(\mathcal{F}_d + \mathcal{F}_{\text{el}})}{\delta \mathbf{n}}. \quad (7)$$

In the literature, the notion ‘‘molecular field’’ is common for $\mathbf{h}(\mathbf{r})$ [2]. Taking the cross product of Eq. (6) with \mathbf{n} one arrives at the vector equation $\mathbf{n} \times \mathbf{h} = \mathbf{0}$ (‘‘balance of torques’’), where the three components are not linearly independent. Thus, keeping the y and the z components one arrives at the standard director equations:

$$h_z n_x - h_x n_z = 0, \quad h_y n_x - h_x n_y = 0. \quad (8)$$

The explicit expressions for the components of \mathbf{h} can be found in Appendix A.

Using the ansatz Eq. (1) for \mathbf{E} in Eq. (4), one easily obtains

$$\frac{\delta \int d^3\mathbf{r} \mathcal{F}_{\text{el}}}{\delta \phi} = \text{div } \mathbf{D} = 0. \quad (9)$$

Here, \mathbf{D} denotes the dielectric displacement

$$\mathbf{D} = \epsilon_0[\epsilon_{\perp} \mathbf{E} + \epsilon_a \mathbf{n}(\mathbf{n} \cdot \mathbf{E})] + \mathbf{P}_{\text{fl}}. \quad (10)$$

The explicit expression of $\text{div } \mathbf{D} = 0$, which means the absence of true charges, can be found in Appendix A.

As a consequence, the equilibrium solutions for \mathbf{n} and ϕ have to satisfy Eqs. (8) and (9). To guarantee $\mathbf{n}^2 = 1$, we use the ansatz $n_x = 1 - \delta n_x$, which leads to

$$\delta n_x^2 - 2\delta n_x + n_y^2 + n_z^2 = 0 \quad (11)$$

or

$$\delta n_x = 1 - \sqrt{1 - n_y^2 - n_z^2}. \quad (12)$$

In our analysis, the extensions of the integration domain in space are chosen as L_x , L_y , L_z , where $L_x, L_y \gg L_z = d$. In the x and y directions we require periodic boundary condition, while δn_x , n_y , n_z , and ϕ have to vanish at $z = \pm d/2$.

For the flexodomains \mathbf{n} and ϕ depend only on y and z . Then \mathcal{F}_{tot} is also invariant against the reflection $y \rightarrow -y$, which implies

$$\begin{aligned} n_x(-y, z) &= r_y n_x(y, z), \\ n_z(-y, z) &= r_y n_z(y, z), \\ \phi(-y, z) &= r_y \phi(y, z), \\ n_y(-y, z) &= -r_y n_y(y, z), \end{aligned} \quad (13)$$

with a symmetry factor $r_y = \pm 1$. It will be demonstrated in the following sections that the flexodomains are characterized by $r_y = 1$ in Eq. (13).

To fulfill the boundary conditions of \mathbf{n} and ϕ , we use a Galerkin method. It implies Fourier expansions of all fields with respect to y and in the z direction an expansion in terms of suitable trigonometric functions $S_m(z) = \sin[m\pi(z/d + 1/2)]$, which vanish at $z = \pm d/2$. Thus, one uses for $n_y(y, z)$ the ansatz

$$n_y(y, z) = \sum_{k=1}^K \sum_{m=1}^M \hat{n}_y(k, m) \sin(kpy) S_m(z). \quad (14)$$

The fields δn_x , n_z , and ϕ are represented in analogy to Eq. (14), except that the y dependence is described by $\cos(kpy)$. In addition, it turns out that for ϕ and δn_x only the expansion coefficients for even $k = 0, 2, 4, \dots$ have to be kept, while for n_y and n_z only the odd ones, $k = 1, 3, 5, \dots$ contribute. Systematically increasing the cutoffs of the sums, we found that the choice $K = 6$, $M = 8$ was sufficient to guarantee a relative error of less than 0.1% for all numerical data given in this paper.

As usual, all equations will be nondimensionalized. Lengths will be measured in units of d/π and \mathbf{E} in units of $E_0 > 0$. The elastic constants k_{ii} will be given in units of $k_0 = 10^{-12}$ N and the flexocoefficients in units of $\sqrt{k_0 \epsilon_0}$. The free energy will be measured in units of $k_0 L_x$. The main dimensionless control parameter R reads as

$$R = \frac{\epsilon_0 E_0^2 d^2}{k_0 \pi^2} = \frac{\epsilon_0 U^2}{k_0 \pi^2}, \quad (15)$$

where $\epsilon_0/k_0 = 8.8542 \text{ V}^{-2}$. From now on all equations will be given in dimensionless units.

III. REMARKS ON THE LINEAR STABILITY ANALYSIS

While the total free energy, F_{tot} , is always zero for the ‘‘ground-state’’ solution with $\mathbf{n} = \mathbf{n}_0$ and arbitrary $\mathbf{E} = E_0 \mathbf{e}_z$, it becomes negative at a certain critical field strength $E_0 = E_c \propto \sqrt{R_c}/d$, where the bifurcation to the stationary flexodomains with wave number p_c takes place. In the linear regime, only the elastic constants k_{11} and k_{22} come into play and it is convenient to introduce their average value, k_{av} , and their relative deviation, δk , from k_{av} as follows [7]:

$$k_{11} = k_{\text{av}}(1 + \delta k), \quad k_{22} = k_{\text{av}}(1 - \delta k), \quad (16)$$

where obviously $|\delta k| < 1$. We also use instead of the dielectric anisotropy ϵ_a and of the main control parameter R [Eq. (15)] the dimensionless parameter combination μ and the dimensionless voltage u :

$$\mu = \frac{\epsilon_a k_{\text{av}}}{(e_1 - e_3)^2}, \quad u = \frac{|e_1 - e_3|}{k_{\text{av}}} \sqrt{R}. \quad (17)$$

Flexodomains exist for u above the *neutral curve* $u_N(p)$. The minimum of $u_N(p)$ at $p = p_c$ yields the critical (dimensionless) voltage $u_c = u_N(p_c)$, where all quantities depend on δk and μ . For the calculations of $u_N(p)$ we refer to Refs. [7,8]. Some details can be also found in Appendix B. Within the TPA ($\delta k = \mu = 0$, $e_1 + e_3 = 0$) one obtains directly the following well-known expression for the neutral curve $u_N(p)$ [6]:

$$u_N(p) = (p^2 + 1)/p, \quad (18)$$

with its critical point at

$$u_c = 2, \quad p_c = 1. \quad (19)$$

For a fixed u the necessary condition $u > u_N(p)$ restricts the range of possible wave numbers p of the flexodomains to the interval $p_1^N < p < p_2^N$ with

$$p_{1,2}^N = (u \mp \sqrt{u^2 - 4})/2. \quad (20)$$

In the following along with u also its reduced version ε will be used:

$$\varepsilon = u/u_c - 1. \quad (21)$$

Then Eq. (18) transforms into

$$\varepsilon_N(p) = (p - 1)^2/(2p), \quad (22)$$

which yields directly the typical parabolic shape of $\varepsilon_N(p)$ near $p = p_c = 1$. For $p \gg p_c$, $\varepsilon_N(p)$ approaches a straight line with the slope $1/2$.

IV. FLEXODOMAINS IN AND BEYOND THE TERENT'EV-PIKIN APPROXIMATION

As evident from the lengthy, nonlinear expressions for the molecular fields h_x , h_y , h_z , and $\text{div } \mathbf{D}$ [Eqs. (A4) and (A6) in Appendix A], solving Eqs. (8) and (9) is in general a difficult numerical task. Apparently, a great simplification is achieved by the TPA in Ref. [9], already alluded to in the introduction. First, using the one-elastic-constant approximation $k_{11} = k_{22} = k_{33} = k_{\text{av}}$, the lengthy contributions to the molecular field proportional to $(k_{22} - k_{33})$ vanish [see Eqs. (A4) in Appendix A]. Furthermore, the requirements $\varepsilon_a = \varepsilon_{\parallel} - \varepsilon_{\perp} = 0$ and $e_1 + e_3 = 0$ lead to additional simplifications also in the equation for the electric potential ϕ [Eq. (A6) in Appendix A]. In the following, the rescaled control parameter u [Eq. (17)] will be used instead of R in Appendix A.

A closer look at the resulting equations for \mathbf{n} and ϕ shows that the y dependence of all fields is surprisingly simple. In fact, they are solvable, in general, by the ansatz:

$$\mathbf{n} = [\sqrt{1 - f^2(z)}, f(z) \sin(py), f(z) \cos(py)], \quad (23)$$

which shares the y dependence with the linear solution [see Eq. (B2) in Appendix B]. Note that $n_x = \sqrt{1 - f^2(z)}$ results from $\mathbf{n}^2 = 1$. As a consequence of $n_x^2 < 1$, the condition $|f(z)| < 1$ must be valid in general in the (u, p) parameter space for $u > u_c = 2$. If the ansatz for \mathbf{n} above is used in Eq. (A6), ϕ is found to be y independent as well. At the end, the general Eqs. (8) and (9) transform thus into the following coupled nonlinear ODEs for $f(z)$ and the rescaled electric potential $\tilde{\phi} = u\phi(z)$:

$$\begin{aligned} \sqrt{1 - f^2} f'' - (\sqrt{1 - f^2})' f + [C(p, u) \\ - p\tilde{\phi}'] \sqrt{1 - f^2} f = 0, \end{aligned} \quad (24a)$$

$$\tilde{\phi}'' - p\alpha(f^2)' = 0, \quad (24b)$$

where

$$C(p, u) = p(u - p), \quad \alpha = \frac{2e_1^2}{k_{\text{av}}\varepsilon_{\perp}}, \quad (25)$$

with $u = 2|e_1|\sqrt{R}/k_{\text{av}}$ [see Eq. (17)]. Furthermore, in Eqs. (24), as also later in this section, derivatives with respect to z are denoted by a prime. Since n_y , n_z , and $\tilde{\phi}$ have to vanish at $z = \pm\pi/2$, the ODEs for f and $\tilde{\phi}$ [Eqs. (24)] have to be solved with the boundary conditions $f(\pm\pi/2) = \tilde{\phi}(\pm\pi/2) = 0$.

It is easy to see, that Eqs. (24a) and (24b) can be recovered as the functional derivatives $\delta F/\delta f$ and $\delta F/\delta\tilde{\phi}$, respectively, of the free-energy functional:

$$\begin{aligned} F(f, \tilde{\phi}; u, p, \alpha) = \frac{k_{\text{av}}}{2} \int_{-\pi/2}^{\pi/2} dz \left\{ [(\sqrt{1 - f^2})']^2 + (f')^2 \right. \\ \left. - [C(p, u) - p\tilde{\phi}'] f^2 - \frac{1}{2\alpha} (\tilde{\phi}')^2 \right\}. \end{aligned} \quad (26)$$

As it should be, the functional F is identical to the total free energy F_{tot} on the basis of the free-energy density \mathcal{F}_{tot} [Eq. (2)] when using the ansatz for \mathbf{n} in Eq. (23) and the y independence of $\tilde{\phi}$.

Our main goal is to determine the wave number $p = p_{\text{min}}(u)$, where F attains its absolute minimum at fixed u and α . In a first step, we locate the stationary points of F , which requires vanishing functional derivatives $\delta F/\delta f$ and $\delta F/\delta\tilde{\phi}$. This is obviously guaranteed for all solutions $f(z; u, p, \alpha)$, $\tilde{\phi}(z; u, p, \alpha)$ of Eqs. (24). One of these solutions, $f_m(z; u, p, \alpha)$, $\tilde{\phi}_m(z; u, p, \alpha)$, yields then the minimum, $F_m(u, p, \alpha) < 0$, of F , which exists for u above the neutral curve $u_N(p)$ [Eq. (18)] with $p_1^N < p < p_2^N$ [Eq. (20)], i.e., for $C(p, u) > 1$.

The construction of f_m , $\tilde{\phi}_m$ simplifies by the observation that Eqs. (24) are invariant against the transformation $z \rightarrow -z$ with $f(-z) = cf(z)$ and $\tilde{\phi}(-z) = -c\tilde{\phi}(z)$, $c = \pm 1$. In fact, only solutions f_m and $\tilde{\phi}_m$, which belong to the ‘‘even’’ class ($c = 1$) become relevant in our case. Note that in this case $\tilde{\phi}(0) = 0$ holds in agreement with Eq. (27). The prevalence of even $f(z)$ solutions against odd ones with additional nodes is not surprising, since stronger spatial variations of f lead obviously to larger positive contributions to F in Eq. (26).

It is easy to see that Eq. (24b) together with the boundary condition $\tilde{\phi}(z = \pm\pi/2) = 0$ can be reformulated in the special case of even $f(z)$ as follows:

$$\begin{aligned} \tilde{\phi}(z) = \alpha p \left[\int_{-\pi/2}^z d\bar{z} f^2(\bar{z}) \right. \\ \left. - \frac{1}{\pi} \left(z + \frac{\pi}{2} \right) \int_{-\pi/2}^{\pi/2} d\bar{z} f^2(\bar{z}) \right]. \end{aligned} \quad (27)$$

Thus, $\tilde{\phi} \equiv 0$, as part of the TPA in Ref. [9], corresponds formally to the limit $\alpha \rightarrow 0$.

A detailed discussion of Eqs. (24) in the nonlinear regime is found in Appendix D. In the special case, $\tilde{\phi} = 0$ ($\alpha = 0$), Eq. (24a) allows for an analytical even-in- z solution $f_m(z)$. The same symmetry governs also the case $\alpha \neq 0$, where Eqs. (24) are numerically solved using standard ODE-solvers.

In general, we exploit the fact that the derivative $\partial_p F_m(u, p, \alpha)$ has to vanish for $p = p_{\text{min}}(u)$. One has thus

to solve the equation

$$\frac{\partial F_m}{\partial p} = -\frac{k_{av}}{2} \left\{ (u - 2p)I[f_m^2] - I[\tilde{\phi}'_m f_m^2] \right\} = 0, \quad (28)$$

where

$$\begin{aligned} I[f_m^2] &= \int_{-\pi/2}^{\pi/2} dz f_m^2(z), \\ I[\tilde{\phi}'_m f_m^2] &= \int_{-\pi/2}^{\pi/2} dz \tilde{\phi}'_m(z) f_m^2(z). \end{aligned} \quad (29)$$

Note that only the explicit derivatives with respect to p have to be kept because of $\delta F/\delta f_m = \delta F/\delta \tilde{\phi}_m = 0$. Thus, we arrive from Eq. (28) at the implicit relation

$$p_{\min} = u/2 - \Sigma_m(u, p_{\min}, \alpha), \quad (30)$$

where

$$\Sigma_m(u, p_{\min}, \alpha) = \frac{I[\tilde{\phi}'_m f_m^2]}{2I[f_m^2]}. \quad (31)$$

In view of our construction of F_m , it is evident that we have to determine the solutions $p = p_{\min}(u)$ of Eq. (30), which minimize F_m , i.e., $\partial_{pp} F_m(u, p, \alpha) > 0$ holds for the second derivative at $p = p_{\min}(u)$. The determination of $p_{\min}(u)$ requires, in general, a numerical treatment, since Σ_m depends on u , p , and α via solutions f_m and $\tilde{\phi}_m$. For $\alpha = 0$ ($\tilde{\phi} = 0$), however, solving Eq. (30) is trivial and leads to the following linear relation:

$$p_{\min} = u/2, \text{ or } p_{\min} - p_c = (u - u_c)/2 = \varepsilon, \quad (32)$$

without even determining $f_m(z)$ from Eq. (24a). This is one of the central results of this paper. The value of the slope $dp_{\min}/du = 1/2$ disagrees, however, with the one given in Ref. [9] for large $u \gg u_c$, where one finds the value $0.603/\pi = 0.192$ in our units. This discrepancy might first appear as a minor problem. However, as demonstrated in Appendix E, the approximate approach used in Ref. [9] is, in general, not sufficient for large u and suffers also from calculation errors.

In Fig. 1, on the basis of Eq. (30), the curves $p_{\min} - p_c$ as function of $\varepsilon = u/u_c - 1$ are plotted for different α . The

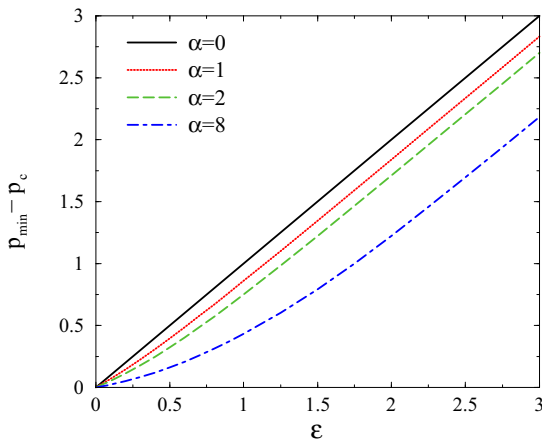


FIG. 1. Plot of $p_{\min} - p_c$ given by Eq. (30) as function of $\varepsilon = u/u_c - 1$ for different values of α .

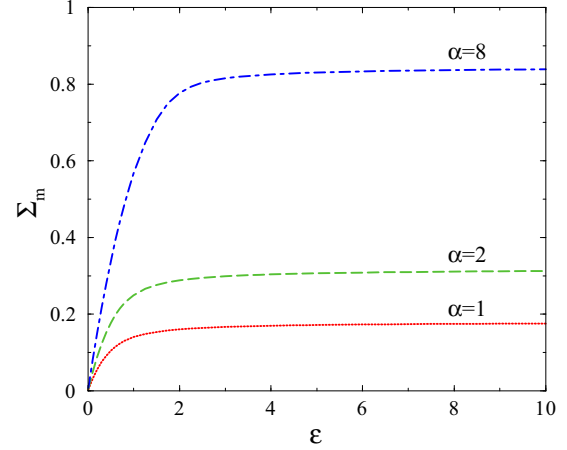


FIG. 2. The downward shift Σ_m [Eq. (31)] of $p_{\min} - p_c$ as function of $\varepsilon = u/u_c - 1$ for different values of α .

straight solid line $p_{\min} - p_c = \varepsilon$ [Eq. (32)] corresponds to $\alpha = 0$ (TPA); the remaining lines are all shifted downwards for finite α . In line with Eq. (30) this vertical shift is given by Σ_m . It first increases with increasing ε but becomes then quickly constant for finite ε . Thus, the slope $dp_{\min}/d\varepsilon$ for larger ε equals again 1, as in the case $\alpha = 0$. To clarify the α dependence of the shift in more detail, Σ_m is plotted in Fig. 2 as function of ε for different α . First, it is obvious that the curves develop quickly an extended plateau as function of ε . With respect to α , the plateau heights increase monotonically as $0.186\alpha^{0.73}$. We have no direct analytical insight into the exponent of α , but according to Appendix D the general trend is qualitatively understood by a rough estimate of the integrals $I[f^2]$, $I[\tilde{\phi}' f^2]$ for $f = f_m(z)$, which determine Σ_m in Eq. (31).

In general, it is also of interest to study the *stability* of the “minimal” solutions \mathbf{n}_m and ϕ_m , where \mathbf{n}_m is given by Eq. (23) with $f(z) = f_m(z)$ at a fixed u for varying p . In particular, we are interested in long-wavelength phase modulations of $\mathbf{n}_m(y, z)$, which lower the free energy F_m . One considers thus a perturbation of the wave number p using the ansatz $p y \rightarrow p y + a \cos(s y)$ with a small amplitude $a \ll 1$ in the limit $s \ll p$. If these phase-modulated solutions lower F_m at a certain p , we speak of an *Eckhaus* instability of the ideally periodic solutions with wave number $p = p_E$. This instability has been studied for many different systems in the literature (for a general discussion, see Ref. [16]). For systems, which are governed by a free energy as in our case, it has been shown in Ref. [17] that the solution $p = p_E$ of $\partial_{pp} F_m(p) = 0$ determines the Eckhaus instability. In our case, one starts from $\partial F_m/\partial p$ in Eq. (28) to arrive at

$$\begin{aligned} \frac{\partial^2 F_m}{\partial p^2} &= -\frac{k_{av}}{2} \left[-2I[f_m^2] \right. \\ &\quad \left. + (u - 2p) \frac{\partial I[f_m^2]}{\partial p} - \frac{\partial I[\tilde{\phi}'_m f_m^2]}{\partial p} \right] = 0. \end{aligned} \quad (33)$$

To determine the solution $p = p_E(u)$ this equation has been analyzed numerically.

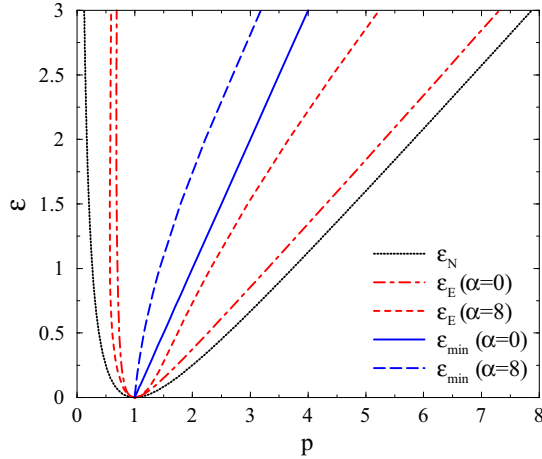


FIG. 3. Phase diagram of flexodomains: neutral curve $\varepsilon_N(p)$, Eckhaus curves $\varepsilon_E(p)$, and $\varepsilon_{\min}(p)$ curves for $\alpha = 0$ and $\alpha = 8$.

Finally, we present in Fig. 3 the complete phase diagram of flexodomains in the p, ε plane for the TPA ($\alpha = 0$) and for $\alpha = 8$, where similar to Fig. 1 the reduced control parameter $\varepsilon = u/u_c - 1$ is used. Flexodomains exist in a region bounded by the neutral curve $\varepsilon_N(p)$ [Eq. (22)] and are stable in a smaller region bounded by the Eckhaus curve $\varepsilon_E(p)$. Furthermore, we show also some representative curves for $\varepsilon_{\min}(p)$, the inverse function of $p_{\min}(\varepsilon)$ in Fig. 1. They appear as straight lines except near $p = p_c = 1$, i.e., near $\varepsilon = 0$.

In general, with increasing α the impact of the induced potential ϕ on the phase diagram becomes more and more pronounced. Thus, it is obvious that the ad hoc approximation $\phi \equiv 0$ in Ref. [9] is rather poor.

The numerical calculations of the phase diagram in Fig. 3 are well confirmed by the much simpler weakly nonlinear analysis for $u \gtrsim u_N(p)$, as described in Appendix C. Here Eqs. (24) are solved with the standard ansatz $f(z) = A \sin(z + \pi/2)$, which is based on the linear solution near onset. The amplitude A is shown to converge to zero in the limit $u \rightarrow u_N(p)$ with $C(p, u_N(p)) \rightarrow 1$. Thus, the bifurcation of flexodomains from the planar basic state is continuous in agreement with the experiments. The total free energy is approximated by a quartic polynomial in A , which allows the calculation of $\varepsilon_{\min}(p)$ and $\varepsilon_E(p)$ in the weakly nonlinear regime. As detailed in Appendix C, the resulting data match well the exact numerical ones.

V. FLEXODOMAINS IN REAL NEMATICS: EXPERIMENTS AND THEORY

The previous section was devoted to a theoretical analysis of flexodomains using the special parameter set convention of the TPA, which allowed even for analytical solutions. Thus, a first insight into the main features of flexodomains in the nonlinear regime has already been achieved.

In this section, we will analyze flexodomains for more general, realistic material parameters, which require a full numerical solution of the basic equations. Instead of systematic studies of parameter variations, which would go beyond the scope of this paper, we will restrict ourselves to selected nematics,

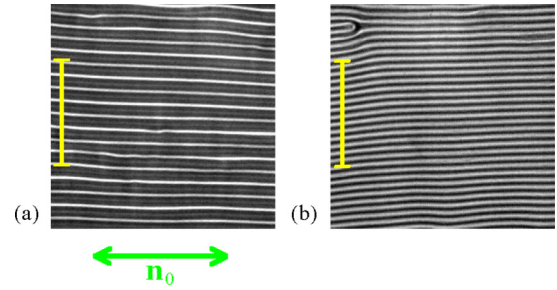


FIG. 4. Shadowgraph images of flexodomains recorded at two different applied voltages for the nematic Phase 4. (a) $U^{\text{exp}} - U_c^{\text{exp}} = 7$ V; (b) $U^{\text{exp}} - U_c^{\text{exp}} = 27$ V. The length of the scale bar is $50 \mu\text{m}$, the double arrow indicates the initial director orientation \mathbf{n}_0 . The cell thickness is $d = 10.8 \mu\text{m}$.

which have not shown electroconvection under an applied dc voltage and where the material parameters are known to some extent. In detail we analyze thus experiments in the nematic mixtures Phase 4 [18] and Phase 5 [19,20], the rodlike compound 4-n-octyloxyphenyl 4-n-methoxybenzoate (10O8) [21], and a bent-core nematic 2,5-di4-[(4-heptylphenyl)-difluoromethoxy]-phenyl-1,3,4-oxadiazole (7P-CF₂OODBP) [14].

The measurements have been performed using standard sandwich cells, where rubbed, polyimide-coated electrodes provided a planar initial orientation \mathbf{n}_0 of the director. Flexodomains have been excited by applying a dc voltage U^{exp} to the whole cell, which are then observed in a polarizing microscope using shadowgraphy [22]. Figure 4 shows representative examples of shadowgraph images of flexodomains at two voltages U^{exp} above the threshold value U_c^{exp} . As already mentioned, the flexodomains cannot be confused with electroconvection rolls since the latter show an orientation orthogonal to the initial director alignment. Furthermore, in contrast to electroconvection patterns, flexodomains remain relatively regular even at voltages considerably above threshold, with only a few defects [see the one in Fig. 4(b)].

To determine the threshold voltage U_c^{exp} , we systematically monitor as function of U^{exp} the contrast of the flexodomains patterns, which vanishes, when approaching the flexoelectric instability at U_c^{exp} from above. The wave number $p(U^{\text{exp}})$ of the flexodomains is obtained from a two-dimensional Fourier transformation of the patterns, where the critical wave number p_c^{exp} is determined by $p_c^{\text{exp}} = p(U_c^{\text{exp}})$. The resulting data for the four nematics mentioned before are listed in Table I (for details, see Appendix F). In Fig. 5 we present the experimental data plotted as $p(U^{\text{exp}}) - p_c^{\text{exp}}$ as function of $U^{\text{exp}} - U_c^{\text{exp}}$. Obviously, $p(U^{\text{exp}})$ is quite well described by linear curves. This feature has been already described before in the theoretical studies of Sec. III and has strongly suggested the following analysis.

A direct comparison of the experiments with theory is far from straightforward. The main control parameter in theory is the voltage drop U over the nematic layer. In contrast, the experimental voltage U^{exp} contains in addition the contribution of the boundary layers at the electrodes, which is practically not available. To cope with this problem, we have exploited the empirical fact, that in experiments with the same nematic

TABLE I. Experimental data, material parameters, and theoretical results for the nematics Phase 4, Phase 5, 10O8, and 7P-CF₂OODB. Cell thickness d measured in μm , critical voltage number p_c^{exp} in units of π/d , critical voltage U_c^{exp} in V. The elastic constants in units of k_0 , the dielectric constants in units of ϵ_0 are taken from the literature. Together with $e_1 - e_3$, in units of $\sqrt{k_0\epsilon_0}$ they determine the scaling factor $s = U/u$. The linear stability analysis of the full equations gives then $U_c = s u_c$ in V. For details, see Appendix F.

	Phase 4	Phase 5	10O8	7P-CF ₂ OODB
d	10.8	6.9	10.8	6.0
p_c^{exp}	1.21	1.14	2.35	2.77
U_c^{exp}	13.0	11.0	26.0	22.0
k_{av}	7.5	7.2	5.3	10.6
δk	0.213	0.361	0.302	0
k_{33}	14.1	12.7	8.2	25.6
ϵ_{\perp}	5.0	5.25	4.53	9.5
ϵ_a	-0.1	-0.184	-0.428	-4.3
$e_1 - e_3$	1.88	2.93	1.91	7.69
s	4.2	2.59	2.93	1.45
U_c	10.64	5.97	23.0	12.61

material the values of p_c^{exp} are fairly reproducible for different electrode configurations in distinct contrast to U_c^{exp} . Thus, it is

suggested that p_c^{exp} is mainly determined by the nematic layer alone, which is described by the theory.

For a given material parameter set we have to construct the numerical solutions of the basic equations for \mathbf{n} [Eq. (8)] and ϕ [Eq. (9)], together with the normalization of \mathbf{n} [Eq. (11)]. The linear analysis (see Sec. III and Appendix B) yields p_c and the nondimensional critical voltage u_c . Most material parameters of the four nematics introduced before have been measured except the flexocoefficients e_i . Their difference, $e_1 - e_3$, has been determined for each material by fitting the theoretical values of p_c to the experimental values p_c^{exp} (see Appendix B), such that for each material $p_c = p_c^{\text{exp}}$ holds. The full material parameter sets used in this paper for the four nematics mentioned before are listed in Table I. In the nonlinear regime we make use of Galerkin expansions as defined in Sec. II, whereby we arrive at a system of coupled nonlinear algebraic equations for the Galerkin expansion coefficients, which are solved by Newton's iteration methods. The iterations start from the weakly nonlinear solutions for $u \gtrsim u_N(p)$, which are easily obtained (see Appendix C). As in the previous section, we obtain then the minimal free energy $F_m(u, p)$ on the basis of $F_{\text{tot}} = \int d^3r \mathcal{F}_{\text{tot}}$ with the free-energy density defined in Eq. (2). Solving numerically $\partial_p F_m(u, p) = 0$ yields $p_{\text{min}}(u)$ as function of u , as discussed before [see Eq. (32) for the TPA case]. For this calculation we need also

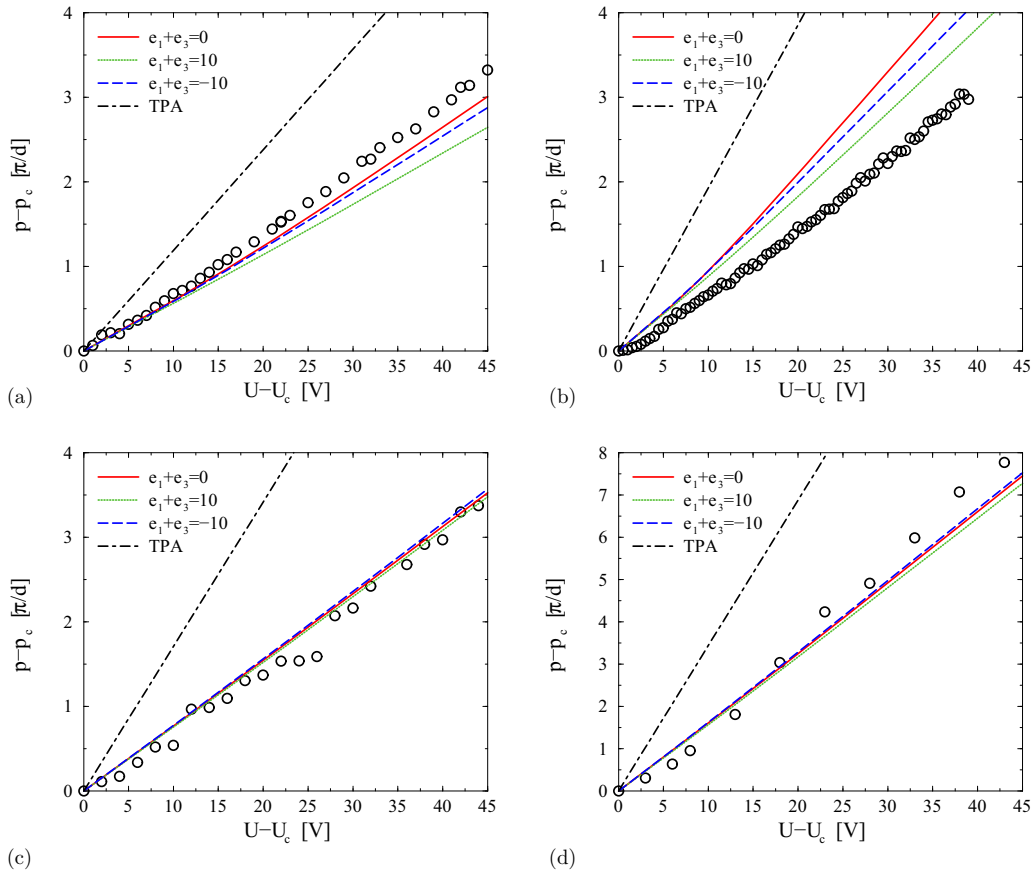


FIG. 5. The reduced wave number of flexodomains $p - p_c$ (in units of π/d) as function of $U - U_c$ (in volts) for various nematics: (a) Phase 4, (b) Phase 5, (c) 10O8, and (d) 7P-CF₂OODB. The open circles correspond to the experimental data, where U corresponds to U^{exp} and p to $p(U^{\text{exp}})$. The straight lines present the corresponding theoretical curves of $p_{\text{min}}(U)$ for the material parameters from Table I and $e_1 + e_3 = 0, \pm 10$. Furthermore, the corresponding TPA curves (dashed-dotted) are plotted as well.

the values of the sum $e_1 + e_3$. Thus, we have compared the solutions for the representative values $e_1 + e_3 = 0, \pm 10$ and found only a quite weak dependence on $e_1 + e_3$. Furthermore, to test the numerical procedure described above, it has been applied also to the TPA case, where indeed all results of Sec. IV have been reproduced.

To compare the theoretical results with the experiments we switch now from the dimensionless voltage u to U measured in volts. According to Eqs. (15) and (17) the corresponding scaling factor s is given as

$$s = \frac{U}{u} = \frac{k_{\text{av}}\pi}{|e_1 - e_3|} \sqrt{\frac{k_0}{\epsilon_0}}. \quad (34)$$

The resulting theoretical data for $p_{\text{min}} - p_c$ (in units of π/d) are then presented in Fig. 5 as a function of the voltage difference $U - U_c$ (in volts). Note that the curves do not depend on d since they derive from the strictly d -independent, dimensionless basic equations in Appendix A. It is evident that the slope dp_{min}/dU remains constant over a wide range of U for all material parameter sets. Furthermore, the dependence of the theoretical curves on $e_1 + e_3$ is indeed weak.

Figure 5 also depicts (as dot-dashed lines) in physical units the corresponding TPA curves for $\delta k = \epsilon_a = e_1 + e_3 = \phi = 0$, where $u_c = 2$, $p_c = 1$ [Eq. (19)]. The material parameters k_{av} and $e_1 - e_3$, listed in Table I, come in only via the scaling factor s in the same table. In physical units we obtain thus $U_c^{\text{TPA}} = 2s$ and the TPA relation Eq. (32) yields $p_{\text{min}} - p_c = (U - U_c^{\text{TPA}})/(2s)$ shown in Figure 5 for the four nematics as function of $U - U_c^{\text{TPA}}$. Note that the TPA leads to significantly larger slopes compared to the exact numerical calculations.

As already mentioned, the nematic layer presents only one part of the experimental cell. Unfortunately, the voltage drop U over this layer, which is provided by the theory is not directly accessible in the experiment. One expects, however, that U should be smaller than U^{exp} due to an internal voltage attenuation in the cell. This attenuation, on the one hand, may originate from the ratio of the impedances of the nematic and of the boundary layers [20]. On the other hand, due to the dc driving, ionic Debye layers may form at the electrodes, which yields a nonuniform initial electric field distribution in the sample reducing the voltage drop over the nematic layer. Inspection of Fig. 5 shows, however, that, apart from Phase 5, the theoretical curves match remarkably well the experimental data. This observation seems to indicate that the difference between U and U^{exp} is fairly independent of U^{exp} . We are unable to give a theoretical foundation of this finding, which is certainly a demanding task, going much beyond the scope of the present paper.

VI. CONCLUSIONS

In this paper we have presented a complete theoretical analysis of flexodomains in planar layers of nematic liquid crystals in the nonlinear regime. Our main focus was on the wave number $p(U)$ of the flexodomains as function of the applied dc voltage U . It is important, that in view of the scaling properties of the basic equations with respect to d (see Appendix A), wave numbers strictly vary as $1/d$ in physical

units, which is in general not the case for electroconvection patterns.

In contrast to the common approach in the literature starting with Ref. [9], which is based on a direct minimization of the free energy, we have concentrated in this paper first on the solution manifold of the basic equations. This gives additional insights and allows for instance a systematic weakly nonlinear analysis near the onset of the flexodomains instability. In particular, in the framework of the approximation used in Ref. [9], we obtain an exact analytical solution of $p(U)$, which is linear in U . In this context it is demonstrated that this often-cited paper is incorrect.

In addition, for four different nematics with well-known material parameters the measurements of the wave number $p(U)$ of the flexodomains and a full numerical analysis have been performed. In all cases, we arrived at a linear relation between p and U . For three of our nematics even the calculated slopes of $p_{\text{min}}(U)$ are in a very good agreement with the experimental ones despite the experimental uncertainties discussed in the previous section. Why the experimental and the theoretical slope of $p(U)$ for the nematic Phase 5 differ more strongly remains open for the moment. As a first step it would for instance be useful to perform detailed measurements on flexodomains for the same material, but for different electrode configurations.

As a byproduct of the analysis, we have access to the detailed director configuration of flexodomains as function of p and U in the nonlinear regime. It is planned to exploit this knowledge to analyze also the optical effects of flexodomains in diffraction experiments and in shadowgraphy.

ACKNOWLEDGMENTS

We thank Ying Xiang and Péter Salamon for their assistance in producing the experimental data and H. Brand for useful discussions. Financial support by the National Research, Development and Innovation Office (NKFIH), Grant No. FK 125134, is gratefully acknowledged by N.É. and Á.B.

APPENDIX A: GENERAL EQUATIONS

According to Sec. II, the equilibrium states of our system are characterized by the vanishing of the *functional derivatives* of the total free energy F_{tot} with respect to the director field $\mathbf{n}(\mathbf{r})$ and the electric potential $\phi(\mathbf{r})$. In the present case the corresponding free energy density \mathcal{F}_{tot} depends only on \mathbf{n} , ϕ , and their first spatial derivatives with respect to $\mathbf{r} = (x, y, z)$. Then the functional derivative, for instance with respect to n_x , reads as follows:

$$h_x \equiv \frac{\delta F_{\text{tot}}}{\delta n_x} = \frac{\partial \mathcal{F}_{\text{tot}}}{\partial n_x} - \partial_i \frac{\partial \mathcal{F}_{\text{tot}}}{\partial n_{x,i}} = 0, \quad (A1)$$

where $i = x, y, z$ and a comma indicates spatial derivatives.

It is convenient to rewrite the elastic contribution \mathcal{F}_d [see Eq. (3)] by using the identity

$$(\mathbf{n} \times \text{curl } \mathbf{n})^2 = (\text{curl } \mathbf{n})^2 - (\mathbf{n} \cdot \text{curl } \mathbf{n})^2, \quad (A2)$$

which holds in the case of $\mathbf{n}^2 = 1$. Thus, we arrive at

$$\mathcal{F}_d = \frac{1}{2}[k_{11}(\text{div } \mathbf{n})^2 + k_{33}(\text{curl } \mathbf{n})^2]$$

$$+ (k_{22} - k_{33})(\mathbf{n} \cdot \text{curl } \mathbf{n})^2]. \quad (\text{A3})$$

Note that in the framework of the TPA, where $k_{22} - k_{33} = 0$, the elastic free energy is only quadratic in \mathbf{n} and in its derivatives, which simplifies the calculations.

In the following, we concentrate on flexodomains, which depend only on y and z . The explicit expressions for h_x obtained from Eq. (A1) and the analogous ones for h_y and h_z , which are needed in the director equations [Eq. (8)], read as follows:

$$\begin{aligned} h_x &= k_{33}(n_{x,yy} + n_{x,zz}) \\ &+ (k_{22} - k_{33})\{-2n_x(n_{y,z} - n_{z,y})^2 \\ &+ n_y[n_{x,z}(2n_{y,z} - n_{z,y}) - n_{x,y}n_{z,z}] \\ &+ n_z[n_{x,y}(2n_{z,y} - n_{y,z}) - n_{x,z}n_{y,y}] \\ &+ n_x n_y(n_{z,yz} - n_{y,zz}) + n_x n_z(n_{y,yz} - n_{z,yy}) \\ &+ n_y^2 n_{x,zz} - 2n_y n_z n_{x,yz} + n_z^2 n_{x,yy}\}, \\ h_y &= k_{11}(n_{y,yy} + n_{z,zz}) + k_{33}(n_{y,zz} - n_{z,yyz}) \\ &+ (k_{22} - k_{33})\{n_x[n_{x,y}n_{z,z} + n_{x,z}(2n_{y,z} - 3n_{z,y})] \\ &+ 2(n_z n_{x,y} - n_y n_{x,z})n_{x,z} \\ &+ n_x^2(n_{y,zz} - n_{z,yz}) + n_x(n_z n_{x,yz} - n_y n_{x,zz})\} \\ &+ \epsilon_a R(-n_z + n_y \phi_{,y} + 2n_z \phi_{,z})\phi_{,y} \\ &+ (e_1 - e_3)\sqrt{R}(-n_{z,y} + n_{z,y}\phi_{,z} - n_{z,z}\phi_{,y}) \\ &+ (e_1 + e_3)\sqrt{R}(n_y \phi_{,yy} + n_z \phi_{,yz}), \\ h_z &= k_{11}(n_{y,yz} + n_{z,zz}) + k_{33}(n_{z,yy} - n_{y,yz}) \\ &+ (k_{22} - k_{33})\{n_x[n_{x,z}n_{y,y} + n_{x,y}(2n_{z,y} - 3n_{y,z})] \\ &+ 2(n_y n_{x,z} - n_z n_{x,y})n_{x,y} \\ &+ n_x^2(n_{z,yy} - n_{y,yz}) + n_x(n_y n_{x,yz} - n_z n_{x,yy})\} \\ &+ \epsilon_a R[-n_y \phi_{,y} + (-2n_z + n_y \phi_{,y} + n_z \phi_{,z})\phi_{,z}] \\ &+ (e_1 - e_3)\sqrt{R}(n_{y,y} + n_{y,z}\phi_{,y} - n_{y,y}\phi_{,z}) \\ &+ (e_1 + e_3)\sqrt{R}(n_y \phi_{,yz} + n_z \phi_{,zz}). \end{aligned} \quad (\text{A4})$$

In line with Eq. (A3), the expressions for h_x , h_y , and h_z simplify considerably in the one-elastic-constant approximation $k_{11} = k_{22} = k_{33}$, where the terms nonlinear in \mathbf{n} in the curly brackets vanish. In addition, in Ref. [9] the special case of $\epsilon_a = 0$ and $e_1 + e_3 = 0$ was considered, where eventually only the flexoelectric contributions $\propto (e_1 - e_3)$ survive.

The electric potential is determined by

$$\frac{\delta \int d^3 \mathbf{r} \mathcal{F}_{\text{el}}}{\delta \phi} = -\partial_i \frac{\partial \mathcal{F}_{\text{el}}}{\partial \phi_{,i}} = \text{div } \mathbf{D} = 0. \quad (\text{A5})$$

In detail, we obtain

$$\begin{aligned} \text{div } \mathbf{D} &= -\epsilon_{\perp} \sqrt{R}(\phi_{,yy} + \phi_{,zz}) \\ &+ \epsilon_a \sqrt{R}\{n_y n_{z,y} + n_z(n_{y,y} + 2n_{z,z}) \\ &- n_y[n_y \phi_{,yy} + (2n_{y,y} + n_{z,z})\phi_{,y} + n_{z,y}\phi_{,z}] \\ &- n_z[n_z \phi_{,zz} + (2n_{z,z} + n_{y,y})\phi_{,z} + n_{y,z}\phi_{,y}] \\ &- 2n_y n_z \phi_{,yz}\} + (e_1 - e_3)(n_{y,y}n_{z,z} - n_{y,z}n_{z,y}) \end{aligned}$$

$$\begin{aligned} &+ (e_1 + e_3)[n_y(n_{y,yy} + n_{z,yz}) \\ &+ n_z(n_{y,yz} + n_{z,zz}) + n_{y,y}n_{z,z} + n_{y,z}n_{z,y} \\ &+ n_{y,y}^2 + n_{z,z}^2] = 0. \end{aligned} \quad (\text{A6})$$

Even using the approximation $\epsilon_a = 0$ and $e_1 + e_3 = 0$, a term $\propto (e_1 - e_3)$, quadratic in the spatial derivatives of \mathbf{n} survives. It results in a finite correction via ϕ to the basic potential $-E_0 z$; however, it has been neglected in Ref. [9]. It should be realized that the thickness of the nematic layer d has perfectly scaled out in the nondimensional Eqs. (A4) and (A6).

APPENDIX B: LINEAR STABILITY ANALYSIS

In the linear regime, Eqs. (8) reduce to

$$h_y = 0, \quad h_z = 0. \quad (\text{B1})$$

They are obtained from Eq. (A4) for $k_{22} - k_{33} = 0$ and $\phi = 0$ and have to be solved [in line with Eq. (14)] using the ansatz

$$n_y = \tilde{n}_y(z) \sin(py), \quad n_z = \tilde{n}_z(z) \cos(py), \quad (\text{B2})$$

where $\tilde{n}_y(\pm\pi/2) = \tilde{n}_z(\pm\pi/2) = 0$ have to be fulfilled. Introducing the new variables μ , δk , and u [see Eqs. (16) and (17)], we arrive at a transcendental equation (see Eq. (12) in Ref. [7]), which determines for fixed p a discrete set of u values that depend on μ and δk . The smallest $u > 0$ determines the neutral curve $u_N(p; \mu, \delta k)$. As explained in Ref. [7], this function can be alternatively calculated using a time-dependent ‘‘viscous’’ generalization of Eqs. (B1). In this way, one obtains the growth rates of flexodomains as function of u , which cross zero at $u = u_N(p)$.

It turns out that $|\delta k|$ is fairly small for the nematic materials used in the experiments discussed in Sec. V. Thus, in line with Ref. [7], it is very useful to analyze Eqs. (B1) first in the limit $\delta k \rightarrow 0$ using the ‘‘one-mode’’ approximation $\tilde{n}_y \propto \sin(z + \pi/2)$, $\tilde{n}_z \propto \sin(z + \pi/2)$. The neutral curve is then given as

$$u_N^2(p) = \frac{(p^2 + 1)^2 - \delta k^2(p^2 - 1)^2}{p^2 + \mu[p^2 + 1 + \delta k(p^2 - 1)]}. \quad (\text{B3})$$

The minimum of $u_N^2(p)$ with respect to p determines the critical wave number $p = p_c$:

$$p_c^2 = \frac{(-1 + \delta k^2)\mu + \sqrt{(1 + \delta k)[1 + \delta k(1 + 4\mu)]}}{(1 + \delta k)[1 + \mu(1 + \delta k)]}. \quad (\text{B4})$$

In general, Eqs. (B3) and (B4) approximate very well the corresponding rigorous data. The relative errors are in fact smaller than 0.5% for $|\delta k| < 0.2$; for larger $|\delta k|$, these approximations provide valuable starting conditions for the full numerical analysis for arbitrary δk .

As explained in Sec. V we obtain $e_1 - e_3$ by fitting p_c to p_c^{exp} . The solution of Eq. (B4) with respect to μ defines the function $\tilde{\mu}(p_c)$ as follows:

$$\tilde{\mu}(p_c) = -\frac{(1 + \delta k)(p_c^4 - 1)}{[1 + p_c^2 + \delta k(p_c^2 - 1)]^2}, \quad (\text{B5})$$

from which we obtain $\mu_c^{\text{exp}} = \tilde{\mu}(p_c^{\text{exp}})$. Exploiting then the equation

$$\frac{\epsilon_a k_{\text{av}}}{(e_1 - e_3)^2} = \mu_c^{\text{exp}} \quad (\text{B6})$$

[see Eq. (17)], one obtains for a given value of p_c^{exp} the value of $(e_1 - e_3)^2$ in the one-elastic-constant approximation. That fit is then iteratively refined for arbitrary δk by using the exact solutions of Eq. (B1).

APPENDIX C: WEAKLY NONLINEAR ANALYSIS

In this section we discuss $p_{\min}(u)$ in the so-called weakly nonlinear analysis using the TPA parameters convention $k_{11} = k_{22} = k_{33} = k_{\text{av}}$, $\epsilon_a = 0$, and $e_1 + e_3 = 0$ but keeping $\tilde{\phi}$ finite. One starts with the ansatz $f(z) = A \sin(z + \pi/2)$ in Eqs. (24), which is even in z . It derives from the identical z -dependence of the linear solutions $n_y(y, z)$ and $n_z(y, z)$ of Eqs. (B1) on the neutral curve $u_N(p) = (p^2 + 1)/p$ [Eq. (18)], where $C[p, u = u_N(p)] = 1$ holds. Expanding Eqs. (24) up to cubic order in the amplitude A , which involves also a contribution $\propto A^2$ to $\tilde{\phi}$, we obtain after a simple calculation from the free energy F [Eq. (26)] the corresponding F^{weak} in the weakly nonlinear approximation as

$$F^{\text{weak}} = -\frac{\pi k_{\text{av}}}{4} \left\{ A^2 [C(p, u) - 1] - \frac{A^4}{4} (1 + \alpha p^2/2) \right\}. \quad (\text{C1})$$

Thus, the condition $\partial F^{\text{weak}}/\partial A = 0$ yields the amplitude $A_{\text{eq}}(u, p, \alpha)$ as

$$A_{\text{eq}}^2(u, p, \alpha) = 2 \frac{C(p, u) - 1}{1 + \alpha p^2/2}. \quad (\text{C2})$$

Obviously, since A_{eq}^2 increases continuously with increasing $u > u_N(p)$, i.e., with $C(p, u) > 1$, we have a continuous bifurcation to flexodomains at $u = u_N(p)$. Substituting $A^2 = A_{\text{eq}}^2$ into Eq. (C1) we obtain the equilibrium free energy $F_{\text{eq}}^{\text{weak}}(p, u, \alpha)$ as

$$F_{\text{eq}}^{\text{weak}}(p, u, \alpha) = -\frac{\pi k_{\text{av}}}{4} \frac{[p(u - p) - 1]^2}{1 + \alpha p^2/2}. \quad (\text{C3})$$

Evaluating $\partial_p F_{\text{eq}}^{\text{weak}}(p, u, \alpha) = 0$, one arrives at the relation $p = p_{\min}(u)$, which is written in analogy to Eq. (30) as follows:

$$p_{\min}(u) = u/2 - \Sigma_m(p_{\min}, \alpha), \quad (\text{C4})$$

where

$$\Sigma_m(p_{\min}, \alpha) = \alpha p_{\min} (p_{\min}^2 - 1)/4. \quad (\text{C5})$$

For $\alpha = 0$, one recovers the general linear function $p_{\min}(u) = u/2$ in Eq. (32), which is shifted downwards for $\alpha \neq 0$ and $u > u_c$ consistent with Fig. 1.

In the weakly nonlinear regime, the Eckhaus stability line $u_E(p)$ is determined by $\partial_{pp} F_{\text{eq}}^{\text{weak}}(p, u, \alpha) = 0$, where $F_{\text{eq}}^{\text{weak}}$ is given in Eq. (C3). One arrives at a lengthy expression not shown here. In leading order in α and keeping only terms up

to order $(p - 1)^3$, it reduces to

$$\begin{aligned} \varepsilon_E(p) &= u_E(p)/u_c - 1 \\ &= \frac{3}{2}(p - 1)^2 [1 - (3 - 4\alpha/3)(p - 1)]. \end{aligned} \quad (\text{C6})$$

One sees, in particular, that the $\varepsilon_E(p)$ curve for $\alpha > 0$ runs above the one for $\alpha = 0$ for $p > p_c = 1$ and below for $p < 1$, i.e., the stability region is tilted to the left in agreement with Fig. 3.

APPENDIX D: DISCUSSION OF THE SOLUTIONS

$f(z)$ AND $\tilde{\phi}(z)$

In the following, we discuss Eqs. (24) at first neglecting the $\tilde{\phi}$ correction of the applied field, as done in the work of Terent'ev and Pikin [9], without any comment. It will be demonstrated that in this case the highly nonlinear ODE [Eq. (24a)] for $f(z)$ can be solved in terms of an elliptic function. In view of $|f(z)| < 1$ we use the ansatz $f(z) = \sin[\theta(z)]$ with $\theta(\pm\pi/2) = 0$. Then Eq. (24a) transforms into

$$\partial_{zz}\theta + C(p, u) \sin\theta \cos\theta = 0, \quad (\text{D1})$$

where $C(p, u) = p(u - p)$ and $|f(z)| < 1$ implies $|\theta(z)| < \pi/2$. Multiplication of Eq. (D1) with $\partial_z\theta$ leads to the conservation law:

$$(\partial_z\theta)^2 + C(p, u) \sin^2\theta = \text{const}. \quad (\text{D2})$$

Again we need only even $f(z)$, which implies $\partial_z f(z=0) = 0$ and consequently $\partial_z\theta(z=0) = 0$. Thus, we obtain from Eq. (D2) the condition $C(p, u) \sin^2[\theta(0)] = \text{const}$, which leads via separation of variables to

$$z = -\frac{\pi}{2} + \frac{1}{\sqrt{C} \sin\theta_0} \int_0^\theta d\psi \frac{1}{\sqrt{1 - \sin^2\psi/\sin^2\theta_0}}, \quad (\text{D3})$$

with $\theta_0 = \theta(0)$. The integral over ψ defines the elliptic integral of the first kind, $F(\theta | m)$, with $m = 1/\sin^2\theta_0$ (see, e.g., Chapter 17 in Ref. [23]). Thus, $\theta(z)$ can be expressed by the inverse function $F^{-1}(\theta | m)$. Since $f(z) = \sin[\theta(z)]$, it is convenient to introduce the Jacobi elliptic function $\text{sn}(z | m)$ defined as $\text{sn}(z | m) = \sin[F^{-1}(z | m)]$. Using the general relation $\text{sn}(x | m) = m^{-1/2} \text{sn}(x m^{-1/2} | m^{-1})$, we obtain

$$f(z) = f_0 \text{sn}[(z + \pi/2)\sqrt{C(p, u)} | f_0^2], \quad (\text{D4})$$

with $f_0 = f(z=0)$, which for $z=0$ leads to the following transcendental equation to determine $f_0 = \sin\theta_0$ as function of $C(p, u)$:

$$\text{sn}[(\pi/2)\sqrt{C(p, u)} | f_0^2] = 1. \quad (\text{D5})$$

This equation has to be solved numerically. Here and also in the following *Mathematica* has been extensively used.

From a numerical point of view it is sometimes more convenient to determine first f_0 as function of C by using the inverse function, $\text{sn}^{-1}(x | f_0^2)$, of $\text{sn}(x | f_0^2)$ with respect to the first argument. In particular, $\text{sn}^{-1}(x = 1 | f_0^2)$ defines the complete elliptic integral of the first kind, $K(m)$, with $m = f_0^2$ (see Eq. (17.3.1) of Ref. [23]). Thus, we obtain from Eq. (D5) the relation

$$\frac{\pi}{2} \sqrt{C(p, u)} = K(f_0^2). \quad (\text{D6})$$

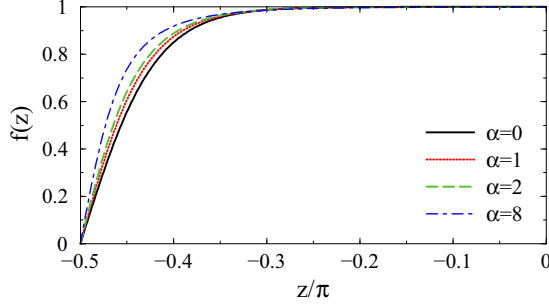


FIG. 6. Solutions $f(z)$ of Eq. (24) for $u = 8$ ($\varepsilon = 3$), $p = p_{\min}(u)$, and different values of α . Since $f(z)$ is mirror symmetric about $z = 0$, it is not shown in the interval $0 \leq z \leq \pi/2$.

Using the limits of $K(m)$ at $m = 0$ and $m = 1$, respectively, to be found again in Ref. [23], we obtain $f_0 \rightarrow 0$ for $C(p, u) \rightarrow 1$ and $f_0 \rightarrow 1$ for $C(p, u) \rightarrow \infty$. As a representative example, the function $f(z)$ is shown in Fig. 6 for $u = 8$ ($\varepsilon = 3$) and $p = p_{\min}(u)$ for different values of α .

In general, $f(z)$ rises with a slope $\propto \sqrt{C}$ at $z = -\pi/2$ and transforms into an extended flat plateau with $f(z) \approx f_0$, when increasing z toward $z = 0$. This observation leads to a rough argument, why the downward shift of $p_{\min}(\varepsilon)$ in Fig. 1 for finite α becomes constant for larger ε . According to Eq. (30) we have to discuss the integrals $I[f^2]$ and $I[\tilde{\phi}' f^2]$. It is obvious that the first one is governed by the plateau regime of $f(z)$ for large C ; thus, $I[f^2]$ approaches π . To estimate $I[\tilde{\phi}' f^2]$, first, Eq. (24b) is integrated with respect to z , which yields

$$\tilde{\phi}'(z) = \alpha p \left[f^2(z) - \frac{1}{\pi} \int_{-\pi/2}^{\pi/2} dz f^2(z) \right]. \quad (\text{D7})$$

Here the condition $\int_{-\pi/2}^{\pi/2} dz \tilde{\phi}'(z) = 0$ has been exploited, which derives from $\tilde{\phi}(\pm\pi/2) = 0$. Using Eq. (D7), the integral $I[\tilde{\phi}' f^2]$ can be rewritten as

$$I[\tilde{\phi}' f^2] = \alpha p \left[\int_{-\pi/2}^{\pi/2} dz f^4(z) - \frac{1}{\pi} (I[f^2])^2 \right]. \quad (\text{D8})$$

For larger C , only the contribution $\propto \alpha p / \sqrt{C}$ from the linear part of $f(z)$ near $z = \pm\pi/2$ survives, while the plateau of $f(z)$ does not contribute. Since $C = O(p^2)$ at large ε , the shift Σ_m becomes indeed ε independent.

APPENDIX E: COMMENT ON THE TERENT'EV AND PIKIN ANALYSIS

The starting point in Ref. [9] was the free-energy density \mathcal{F}_{tot} [Eq. (2)] under the TPA. The condition $\mathbf{n}^2 = 1$ was guaranteed by representing \mathbf{n} in terms of polar angles $\theta(y, z)$, $\varphi(y, z)$:

$$n_x = \cos \theta \cos \varphi, \quad n_y = \cos \theta \sin \varphi, \quad n_z = \sin \theta. \quad (\text{E1})$$

This representation for \mathbf{n} was then substituted into \mathcal{F}_{tot} , where only the terms up to sixth order in θ and φ have been kept.

In addition, θ and φ have been expanded as follows:

$$\begin{aligned} \theta(y, z) &= \cos(\pi z/d) [\theta_1 \cos(py) + \theta_3 \cos(3py)], \\ \varphi(y, z) &= \cos(\pi z/d) [\varphi_1 \cos(py) + \varphi_3 \sin(3py)]. \end{aligned} \quad (\text{E2})$$

After integrating \mathcal{F}_{tot} over z and y , one arrives at the total free energy, $F^{\text{TP}}(\theta_i, \varphi_i)$, in the form of a polynomial of sixth order in θ_i and φ_i , $i = 1, 3$ with coefficients depending on p and u . Next, the solutions $\theta_i(u, p)$, $\varphi_i(u, p)$ of the four coupled nonlinear equations, $\partial F^{\text{TP}}/\partial \theta_i = 0$ and $\partial F^{\text{TP}}/\partial \varphi_i = 0$, $i = 1, 3$, are inserted into F^{TP} . Minimizing the resulting equilibrium free energy $F_{\text{eq}}^{\text{TP}}(p, u)$ at fixed u with respect to p should then give $p_{\min}(u)$ as given in Ref. [9]. Thus, we have carried through the whole procedure using *Mathematica*. Not surprisingly, we obtained in the weakly nonlinear regime ($u \gtrsim u_c = 2$) again $p_{\min}(u) = cu$ with $c = 1/2$. However, while $c = 1/2$ remains unchanged for arbitrary u in our rigorous analytical TPA calculations [see Eq. (32)], it decreases continuously with increasing u in the approximation described above. We find, for instance, $dp_{\min}/du = 0.47$ for $u = 2.5$ and $dp_{\min}/du = 0.31$ for $u = 5$. This finding is in distinct contrast to the corresponding result given in Ref. [9], where $dp_{\min}/du = 0.603/\pi = 0.192$ (in our units) is predicted to hold for large $u \gg u_c$.

That the approximation scheme based on Eq. (E2) is problematic at larger u becomes already clear in the light of our exact solution for \mathbf{n} [Eq. (23)], where, for instance, n_x does not depend on y . Though in Ref. [9] not all details of their calculations are available, their analysis suffers from technical errors. For instance, instead of a required expansion of $\cos^2 \theta (\partial_y \varphi)^2$ term in the elastic part of the free energy expression, erroneously $\cos \theta (\partial_y \varphi)^2$ has been expanded, as inspection of Eq. (2) in Ref. [9] shows. Keeping as a test this error in our calculations, we were even unable to find a minimum of the free energy as function of p for fixed u and must conclude that the analysis in Ref. [9] suffers from additional errors.

APPENDIX F: EXPERIMENTAL AND THEORETICAL DATA AND MATERIAL PARAMETERS

In Table I one finds first some data (cell thickness d , critical wave number p_c^{exp} , and voltage U_c^{exp}) characterizing the experiments in Sec. V together with the corresponding material parameters of our four nematics and the scaling factor $s = U/u$ [Eq. (34)]. The material parameters are taken for the nematic mixture Phase 4 from Ref. [18], for the mixture Phase 5 from Ref. [19], and for the rodlike compound 4-n-octyloxyphenyl 4-n-methyloxybenzoate (1008) from Ref. [21]. Data for the bent-core nematic 2,5-di4-[(4-heptylphenyl)-difluoromethoxy]-phenyl-1,3,4-oxadiazole (7P-CF₂OODBP) [14] are not available, thus those of the similar substance 2,5-di4-[(4-heptylphenyl)-difluoromethoxy]-phenyl-1,3,4-oxadiazole (9P-CF₂OODBP) are taken from Ref. [24]. From the linear stability analysis of the full equations, one obtains $U_c = s u_c$ and p_c , which is identified with p_c^{exp} by fitting $e_1 - e_3$ (see Appendix B).

- [1] N. Éber, P. Salamon, and Á. Buka, *Liq. Cryst. Rev.* **4**, 101 (2016).
- [2] P. G. de Gennes and J. Prost, *The Physics of Liquid Crystals* (Clarendon Press, Oxford, 1993).
- [3] Á. Buka and N. Éber, eds., *Flexoelectricity in Liquid Crystals: Theory, Experiments and Applications* (Imperial College Press, London, 2012).
- [4] Á. Buka, T. Tóth-Katona, N. Éber, A. Krekhov, and W. Pesch, in *Flexoelectricity in Liquid Crystals: Theory, Experiments and Applications*, edited by A. Buka and N. Éber (Imperial College Press, London, 2012), pp. 101–135.
- [5] S. A. Pikin, *Structural Transformations in Liquid Crystals* (Gordon and Breach Science Publishers, New York, 1991).
- [6] Y. P. Bobylev and S. A. Pikin, *Zh. Eksp. Teor. Fiz.* **72**, 369 (1977) [*Sov. Phys. JETP* **45**, 195 (1977)].
- [7] A. Krekhov, W. Pesch, and Á. Buka, *Phys. Rev. E* **83**, 051706 (2011).
- [8] A. Krekhov, W. Pesch, and Á. Buka, *Eur. Phys. J. E* **34**, 80 (2011).
- [9] E. M. Terent'ev and S. A. Pikin, *Zh. Eksp. Teor. Fiz.* **83**, 1038 (1982) [*Sov. Phys. JETP* **56**, 587 (1982)].
- [10] L. K. Vistin', *Kristallografiya* **15**, 594 (1970) [*Sov. Phys. Crystallogr.* **15**, 514 (1970)].
- [11] M. I. Barnik, L. M. Blinov, A. N. Trufanov, and B. A. Umanski, *J. Phys. France* **39**, 417 (1978).
- [12] P. Kumar and K. S. Krishnamurthy, *Liq. Cryst.* **34**, 257 (2007).
- [13] P. Salamon, N. Éber, Á. Buka, T. Ostapenko, S. Dölle, and R. Stannarius, *Soft Matter* **10**, 4487 (2014).
- [14] Y. Xiang, H.-Z. Jing, Z.-D. Zhang, W.-J. Ye, M.-Y. Xu, E. Wang, P. Salamon, N. Éber, and Á. Buka, *Phys. Rev. Appl.* **7**, 064032 (2017).
- [15] L. D. Landau and E. M. Lifshitz, *Electrodynamics of Continuous Media*, Course of Theoretical Physics, Vol. 8 (Pergamon Press, Amsterdam, 1984).
- [16] L. S. Tuckerman and D. Barkley, *Physica D* **46**, 57 (1990).
- [17] L. Kramer and W. Zimmermann, *Physica D* **16**, 221 (1985).
- [18] M. May, W. Schöpf, I. Rehberg, A. Krekhov, and Á. Buka, *Phys. Rev. E* **78**, 046215 (2008).
- [19] T. Tóth-Katona, N. Éber, Á. Buka, and A. Krekhov, *Phys. Rev. E* **78**, 036306 (2008).
- [20] N. Éber, L. O. Palomares, P. Salamon, A. Krekhov, and Á. Buka, *Phys. Rev. E* **86**, 021702 (2012).
- [21] P. Salamon, N. Éber, A. Krekhov, and Á. Buka, *Phys. Rev. E* **87**, 032505 (2013).
- [22] S. Rasenat, G. Hartung, B. L. Winkler, and I. Rehberg, *Exp. Fluids* **7**, 412 (1989).
- [23] M. Abramowitz and A. Stegun, eds., *Pocketbook of Mathematical Functions—Abridged edition of Handbook of Mathematical Functions*, edited by M. Danos and J. Rafelski (Verlag Harri Deutsch, Frankfurt am Main, 1984).
- [24] Y. Xiang, M.-j. Zhou, M.-Y. Xu, P. Salamon, N. Éber, and Á. Buka, *Phys. Rev. E* **91**, 042501 (2015).